Article

A Novel Isolated Intelligent Adjustable Buck-Boost Converter with Hill Climbing MPPT Algorithm for Solar Power Systems

Bushra Sabir [1], Shiue-Der Lu [2], Hwa-Dong Liu [3,*], Chang-Hua Lin [1], Adil Sarwar [4] and Liang-Yin Huang [5]

[1] Department of Electrical Engineering, National Taiwan University of Science and Technology, Taipei 106, Taiwan
[2] Department of Electrical Engineering, National Chin-Yi University of Technology, Taichung 411, Taiwan
[3] Undergraduate Program of Vehicle and Energy Engineering, National Taiwan Normal University, Taipei 106, Taiwan
[4] Department of Electrical Engineering, ZHCET, Aligarh Muslim University, Aligarh 202002, India
[5] Graduate Institute of Manufacturing Technology, National Taipei University of Technology, Taipei 106, Taiwan
* Correspondence: hdliu@ntnu.edu.tw; Tel.: +886-2-7749-5953

Abstract: This study proposes a new isolated intelligent adjustable buck-boost (IIABB) converter with an intelligent control strategy that is suitable for regenerative energy systems with unsteady output voltages. It also serves as a reliable voltage source for loads such as battery systems, microgrids, etc. In addition, the hill climbing (HC) maximum power point tracking (MPPT) algorithm can be utilized with this innovative IIABB converter to capture the MPP and then enhance system performance. In this converter, five inductors (L_A, L_B, L_C, L_D, and L_E) and four power MOSFETs (S_A, S_B, S_C, and S_D) are used in the proposed novel isolated intelligent adjustable buck-boost (IIABB) converter to adjust the applied voltage across the load side. It also has a constant, stable output voltage. The new IIABB converter is simulated and verified using MATLAB R2021b, and the performances of the proposed IIABB converter and conventional SEPIC converter are compared. The solar photovoltaic module output voltages of 20 V, 30 V, and 40 V are given as inputs to the proposed IIABB converter, and the total output voltage of the proposed converter is 48 V. In the new IIABB converter, the duty cycle of the power MOSFET has a small variation. The proposed IIABB converter has an efficiency of 92~99%. On the other hand, in the conventional SEPIC converter, the duty cycle of a power MOSFET varies greatly depending on the relationship between the output and input voltage, which deteriorates the efficiency of the converter. As a result, this research contributes to the development of a novel type of IIABB converter that may be employed in renewable energy systems to considerably increase system performance and reduce the cost and size of the system.

Keywords: isolated intelligent adjustable buck-boost converter; solar power system; hill climbing algorithm; maximum power point tracking; conventional SEPIC converter

1. Introduction

Today, the need for electricity generation from renewable sources is rising for both residential and industrial purposes. Power generation from fossil fuels results in the emission of hazardous substances into the atmosphere. These fossil fuels are declining in the environment over time. Solar energy is one of the most abundant, eco-friendly, and pollution-free renewable energy sources. Using the photovoltaic (PV) effect, a solar cell converts sunlight into electricity. Once a solar energy system is installed, it should be able to operate for an extended period and save money and overall maintenance costs. As a result of its adaptable nature, solar energy can be utilized for a variety of power applications, ranging from little torches to satellites. Conventional energy sources are under imminent threat of extinction. As a result, the new electrical technology is more dependent on non-conventional or renewable energy sources. In the absence of the consistent and continuous output of nonconventional power sources (solar PV, wind turbines, fuel cells, and hybrid

PV/fuel cell/wind turbines), power cannot be sent directly to the load (such as a DC microgrid, a DC home, an electric vehicle, or HVDC transmission, etc.). For charging applications, a high-efficiency and continuous DC–DC power converter is employed to address these disadvantages of renewable energy sources. In addition to PV panels, solar PV systems use power electronic converters to connect their output to the grid or to local loads. DC–DC converters and DC–AC inverters are commonly used power electronics converters. With the MPPT algorithm integrated with the DC–DC converter, the DC–DC converter steps up/down the input voltage of the solar PV array to maximize the power output. Whenever power semiconductor devices are used as switches, electrical interference and power loss are introduced due to the internal resistance of the switches and inductors. It results in a decrease in efficiency and power quality due to these problems. It is imperative to create efficient DC-DC converters and effective MPPT algorithms to mitigate these issues. This paper proposes an isolated intelligent adjustable buck-boost (IIABB) with a coupled inductor wound on a single core for battery charging, which leads to a reduction in the size of the whole setup and hence reduces the current ripple, as discussed in detail. Some applications of the proposed (IIABB) converter are shown in Figure 1.
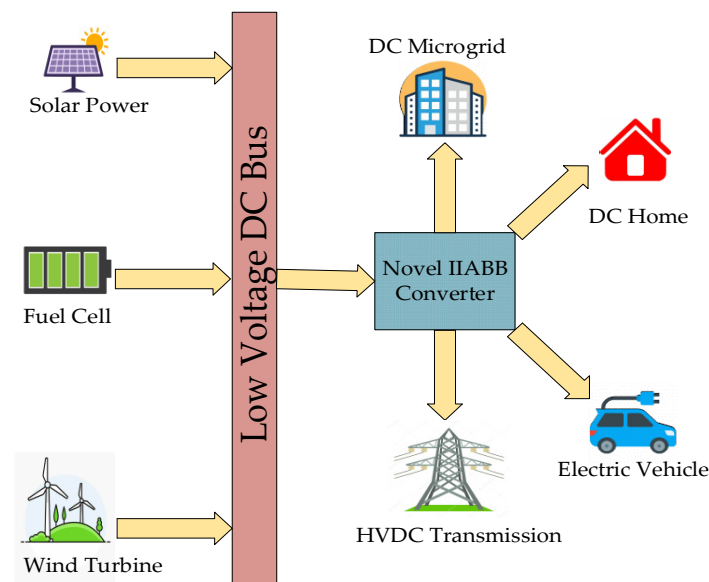

Figure 1. Various applications of the novel IIABB converter.

Various converters exist to satisfy the aforementioned demand; some are discussed here. In a study [1], the author uses a single-ended primary inductance converter (SEPIC) with a passive component in PV systems that require regulated output voltage. The result shows that SEPIC converters are well suited for smooth induction motor speed control. Adaptive nonlinear methods are proposed in [2] for tracking a SEPIC's maximum power point (MPP) and regulating its output voltage. Work [3] employs the bridgeless SEPIC converter for battery charging applications. This system can rectify and convert DC to DC with an improved power factor and low harmonics. In [4], a current sensor-based maximum power point tracking (MPPT) algorithm with adaptive step size is proposed for a solar photovoltaic system based on a SEPIC. Because power is less sensitive to current perturbation than voltage is, the author [5] proposes a high voltage gain SEPIC structure for use in renewable energy applications; such a scheme is seen as a novel SEPIC structure. This shows that the modified SEPIC converter has a higher voltage gain than a conventional SEPIC or the recently discussed single-controlled switch converter. The study [6] presents a novel non-isolated single switch quadratic modified SEPIC converter with high voltage gain. To achieve the suggested, the converter combines a modified SEPIC converter with a boosting module to attain a large voltage gain at a low duty ratio [7], which presents the theory of a new DC-DC power converter's theoretical assessment and numerical

simulations of the SEPIC topology. A three-port dual boost SEPIC converter is described in this article [8] for use in a hybrid PV/battery electric vehicle to enhance the efficiency and capability of the power conversion stage. In this work [9], the perturb and observe (P&O) and incremental conductance (IC) algorithms are used to determine the duty cycle of the SEPIC's pulse width modulation (PWM), which is used to control the system's operation point. The study [10] is centered on the dimensioning and modeling of a continuous conduction mode SEPIC converter. In work [4], the efficiency of standard Boost and SEPIC converters was evaluated and compared to the updated SEPIC converter. This article [11] proposes a simple soft-switching structure adaptable to the various configurations of the modified SEPIC converter, thereby lowering switching losses and diode reverse recovery current. Article [12] utilizes a DC-DC converter with the Cuk-SEPIC configuration, resulting in increased power efficiency and cost savings, especially when used with unnecessary filters. Using a constructed model and a simulink model, this paper [13] compares the conventional SEPIC and cascaded boost–SEPIC converters in detail. This study suggested a new global maximum power point tracking (global-MPPT) method [14]. Under partial shading conditions, the algorithm avoids the P&O technique disturbance problem caused by power points trapped at the local peak point. The work [15] proposes an extendable triple-port SEPIC (TPS) converter as a compact and efficient multiport interface with fewer components for integrating renewable energy sources in a microgrid system. In this publication [16], a PID controller for the SEPIC converter was developed, and the system's performance was investigated when the reference voltage output changed. This study demonstrates that coupling a PID controller to a SEPIC converter is effective in terms of design, analysis, and convenience, as it acts as a step-up and step-down voltage regulator. This article [17] discusses the integration topology of a DC-DC SEPIC converter with a full-bridge DC-AC inverter. The proposed topology can convert the low DC voltage to a higher AC voltage by connecting the circuits in parallel. According to this article [18], the PWM method is used to implement a safe adaptive controller for a non-minimum phase SEPIC converter based on robust adaptive control. The article [19] discusses the comparison of the recently proposed multilevel inverter (MLI). An analysis is conducted in this paper [20] of two proposed models with two distinct modified SEPIC converters, with and without magnetic windings for increased output voltage. In [21], a highly recommended novel maximum power point tracking method is introduced for PV applications derived from the proposed method with the help of the secant incremental gradient method, which is based on the Newton–Rapson method. The moth frame optimizer-perturb and observe method [22] is used to implement the MPPT problem in the PV system. In [23], a hybrid method based on the gray wolf optimizer-crow search algorithm is proposed. This control strategy can efficiently capture the maximum power point under partially shaded and fast-changing irradiance level conditions. The optimization of photovoltaic systems in partial shading conditions is solved with TFWO [24], which is based on the formation of whirlpools in a turbulent flow of water. In order to maximize the power extracted from the photovoltaic system, the optimal duty cycle is determined using the TFWO.

To meet requirements for a constant output voltage from the converter and increase system performance, there needs to be a reduction in the cost and size of the system. A novel type of isolated intelligent adjustable buck-boost (IIABB) converter is introduced.

This paper has been categorized into five sections. The introduction has been discussed in Section 1. Section 2 introduces the conventional SEPIC converter. Section 3 provides a description of the new IIABB converter and HC algorithm. Our simulation and experimental results are presented in Section 4, and in the last section of this paper, conclusions and future directions are presented.

2. Conventional SEPIC Converter

To step down or up the input voltage, such types of converters are used in a buck-boost topology (as shown in Figure 2). The SEPIC produces an output voltage that either exceeds or falls below the input voltage without reversing the polarity. The SEPIC converter

provides the regulated output voltage regardless of whether the input voltage is higher or lower than the constant output voltage. Conventional DC-DC converters are unable to achieve high voltage gain due to their high duty cycles, switching frequencies, transformer requirements, and system size [1–5]. To feed a grid-connected inverter, the low voltage from renewable energy sources must be boosted. The main aim of this paper is to introduce the proposed converters, which are the extended form of this conventional topology.
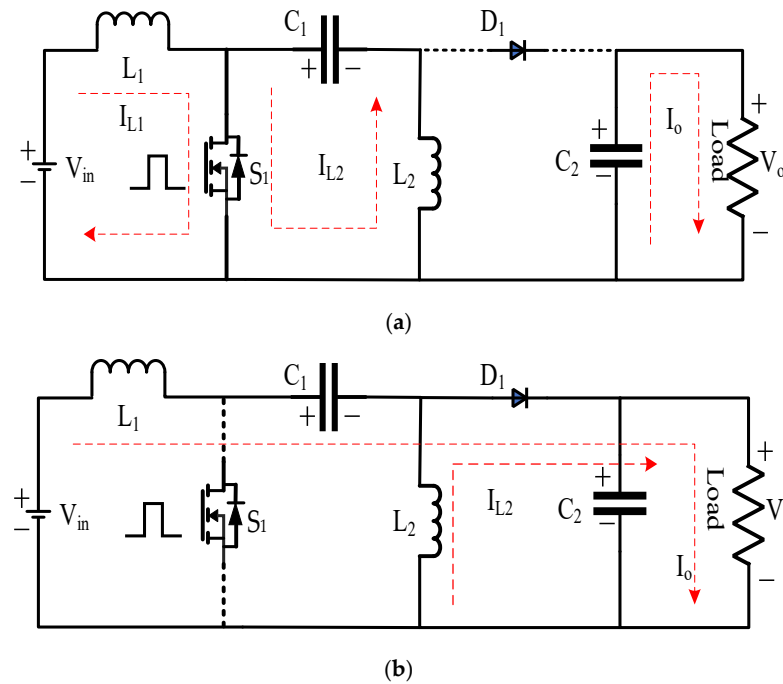

(**a**)

(**b**)

Figure 2. SEPIC Converter's operate mode: (**a**) power MOSFET S_1 during the ON state, (**b**) power MOSFET S_1 during the OFF state.

It is primarily dependent on the duty cycle and parasitic elements in the circuit that determine how much the SEPIC converter steps up or down the level of voltage. The output voltage V_O of the SEPIC converter can be calculated.

$$V_O = \frac{DV_i}{1 - D} \tag{1}$$

where V_i represents the input voltage and D represents the duty cycle.

However, it doesn't contain any parasitic losses such as diode drop losses. Therefore, the equation is as follows:

$$V_O + V_D = \frac{DV_i}{1 - D} \tag{2}$$

This becomes the following:

$$D = \frac{V_O + V_D}{V_i + V_O + V_D} \tag{3}$$

For the continuous conduction mode (CCM) of operation, the computation value of the inductor $L_1 = L_2$ is represented by the equation below:

$$L_1 = L_2 = \frac{V_{imin} + D_{max}}{\Delta i_{omax} + f_{sw}} \tag{4}$$

where, V_{imin} is the absolute minimum voltage that can be fed into the converter, D_{max} represents the maximum duty cycle, f_{sw} represents switching frequency, and Δi_{omax} represents an acceptable output current ripple.

The SEPIC converter is similar to the buck-boost converter, but it has the advantage of having a non-inverting output voltage. A series capacitor is used to transfer energy from a source to a load and is capable of true shutdown. The equivalent circuit of a SEPIC converter, as shown in Figure 2, is as follows: When the switch S_1 is ON, the current I_{L2} starts increasing, and the current across inductor L_1, which comes from the instantaneous voltage source, is approximately equivalent to the input voltage V_{in}, the diode D_1 is opened, the input capacitor C_1 supplies the energy, and it operates according to the waveform during time 0–t_0 as shown in Figure 3. When S_1 is OFF, the current across the capacitor C_1 becomes equal to the I_{L1}, therefore the inductor does not allow instantaneous changes in current. The current flows across the inductor L_2 in a negative direction. This is because if the switch is closed long enough for a half cycle of resonance with inductor L_2, the potential (voltage) across capacitor C_1 will remain the same, which can be seen clearly with the help of the waveform during time t_0–t_1 as shown in Figure 3. Two inductors, L_1 and L_2, a diode D_1, a power MOSFET S_1, an output capacitor C_2, and a coupling capacitor C_1 are used in the converter. Due to the presence of a coupling capacitor with negative polarity, diode D_1 is reverse biased upon activation. When the coupling capacitor discharges, both the inductors L_1 and L_2 get charged. During this time, the diode is turned off, and it becomes forward biased. Inductor L_1 transfers energy to the coupling capacitor, while inductor L_2 delivers energy to the output terminal. The L_1 and L_2 inductors can be coiled on a single core, and they can receive the same switching period voltage. A coupled inductor minimizes the size of the whole circuitry and the overall cost of the system.
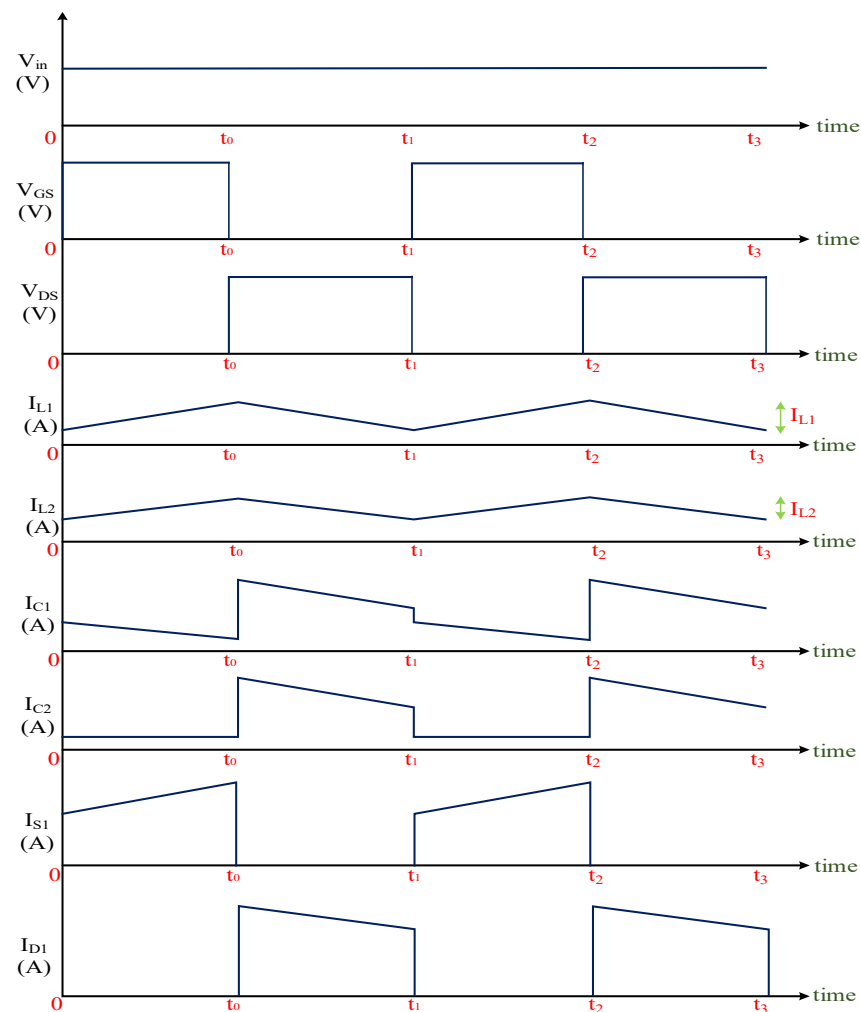

Figure 3. Current and voltage waveforms of a conventional SEPIC converter.

Figure 3 demonstrates the converter switching waveforms. V_{in} is the input voltage across the power MOSFET S_1 when it is turned on and off. I_{S1} represents current across the power MOSFET S_1, I_{C1} represents current across the coupling capacitor, and I_{L1} and I_{L2} inductor currents build linearly. I_{D1} is the diode current, I_{C1} is the current through the coupling capacitor, and I_{C2} is the current through the output capacitor.

3. An Isolated Intelligent Adjustable Buck-Boost Converter Is Proposed

To increase the efficiency of the converter, a modified SEPIC converter is combined with five inductors; in this case, the five inductors are wound on the same core as the coupling design. To reduce ripple current and improve the system's efficiency, and also considering that a high voltage or current can reduce the performance of the SEPIC converter. Five inductors (L_A, L_B, L_C, L_D, and L_E) and four power MOSFETs (S_A, S_B, S_C, and S_D) are used in the proposed novel isolated intelligent adjustable buck-boost (IIABB) converter to adjust the applied voltage across the load side. Its advantage is that this IIABB converter has an intelligent control strategy so that the power MOSFETs (S_B, S_C, and S_D) will not perform high-frequency switching caused by switching loss caused by those power MOSFETs (S_B, S_C, and S_D) only for long ON or OFF times. As a result, the circuit has a different output power. To get the different output, further research can be performed on this design. In the proposed IIABB converter, the power MOSFET S_A stores the output energy of the solar photovoltaic (PV) simulator in the inductor(s) L_A, L_B, L_C, L_D, and L_E. When S_A is ON, the inductor(s) L_A, L_B, L_C, L_D, and L_E energy is transferred to the load side, which actuates the power MOSFETs S_B, S_C, and S_D to further change the output voltage in order to stabilize the output power, as shown in Figure 4; the parameters for the proposed IIABB converter are given in Table 1.
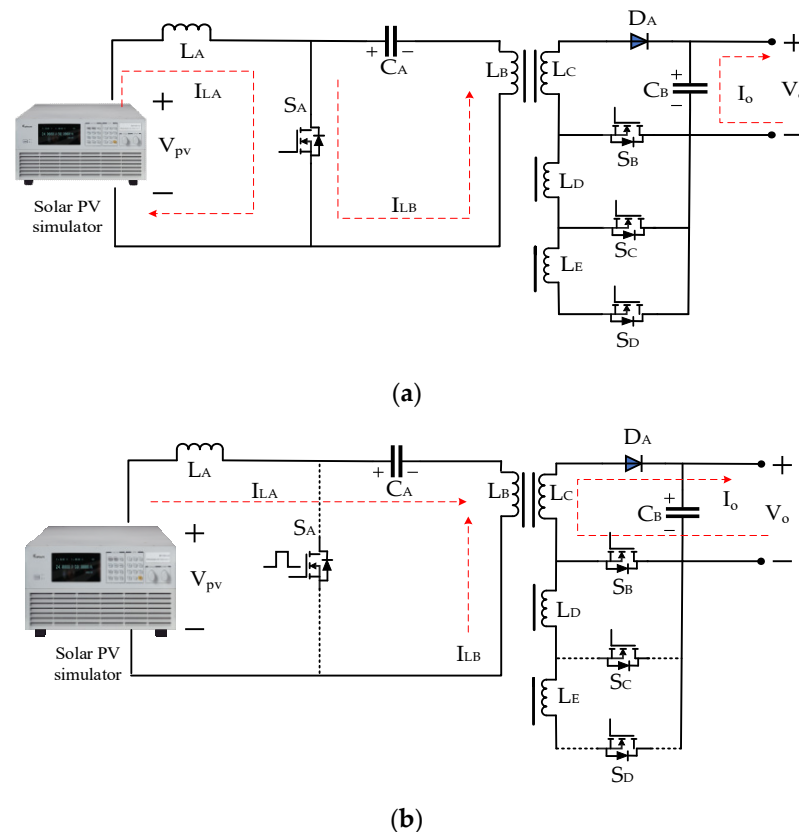

(a)

(b)

Figure 4. *Cont.*
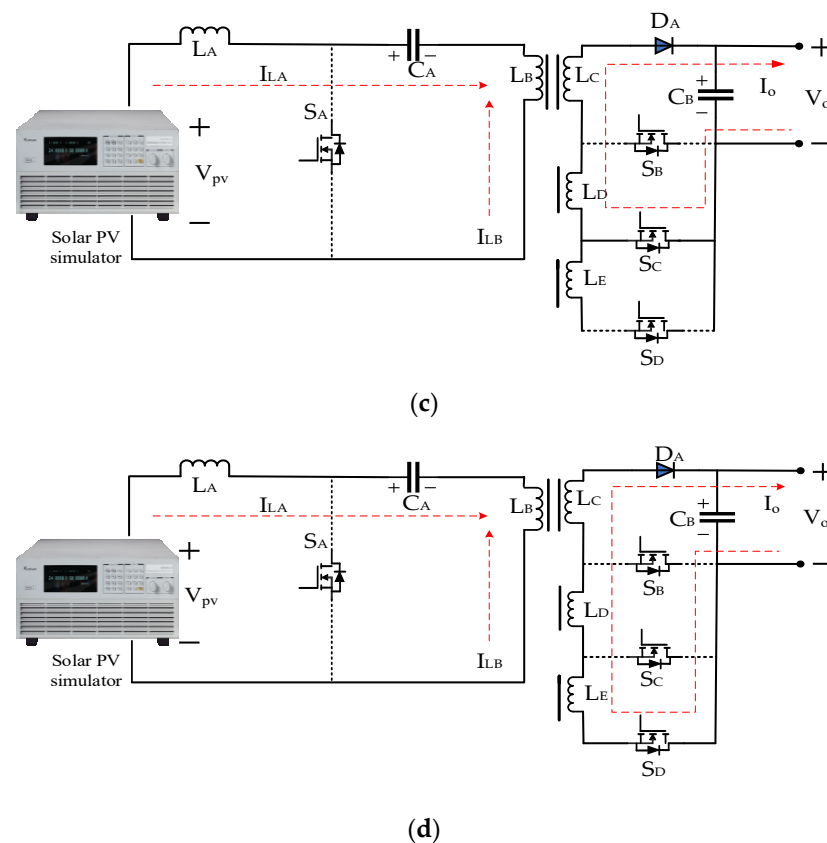
(c)

(d)

Figure 4. Operation of the proposed IIABB converter with an intelligent control strategy: (**a**) the power MOSFET S_A is ON and the power MOSFETs S_B, S_C, and S_D are OFF, (**b**) the power MOSFET S_B is ON and the power MOSFETs S_A, S_C, and S_D are OFF, (**c**) the power MOSFET SC is ON and the power MOSFETs S_A, S_B, and S_D are OFF, and (**d**) the power MOSFET S_D is ON and the power MOSFETs S_A, S_B, and S_C are OFF.

Table 1. The parameters of the proposed IIABB converter.

Component/Parameter	Specification	Quantity
Solar PV simulator output voltage (V_{pv})	20–40 V	–
Switching frequency	20 kHz	–
Rated power	200 W	–
Capacitor (C_A, C_B)	220 µF, 500 µF	2
Inductors (L_A, L_B, L_C, L_D, L_E)	1 mH	5
Output voltage (V_o)	48 V	–

The rising and falling of the output voltage of a conventional SEPIC converter depends on the duty cycle, the input voltage V_{pv}, the diode voltage V_{DA}, the output voltage V_o, and the relationship between the number of connected inductors N and the turn ratio n (taking the turn ratio of 1:1) as expressed by Equation (5) below:

$$V_o = \frac{DV_{pv} - V_{DA}(1 - D)}{1 - D} N \cdot n \tag{5}$$

The circuit diagram of the proposed IIABB converter is shown in Figure 4. The solar PV simulator has an output voltage V_{pv} of 20 V, 30 V, and 40 V and a 48 V constant output voltage, which provides a consistent charging voltage for the various loads.

3.1. Topology Analysis and Intelligent Control Strategy

In this section, various modes of converter have been discussed at different conditions (mode 1, mode 2, and mode 3, respectively) at various duty cycles and numbers of inductors, which are calculated from the output gain Equation (5). The proposed IIABB converter has three working modes described below:

In mode 1 of the proposed IIABB converter combined with an intelligent control strategy, the switch S_A is conducting and the output diode D_A is reverse biased, and no currents will be conducting during this time. The magnetizing inductor L_{MA} from inductor L_A is subjected to a voltage, and its current rises according to Equation (6).

$$I_{LMA}(t) = \frac{V_{pv}(t_1 - t_0)}{L_{MA}} + I_{LMA}(0) \tag{6}$$

The power MOSFET S_A is ON and power MOSFETs S_B, S_C, and S_D are OFF (as shown in Figure 4a), and the proposed IIABB converter operates according to the waveform during time t_0–t_1 as shown in Figure 5. In the next interval of the proposed IIABB converter, the power MOSFET S_B is ON and the power MOSFETs S_A, S_C, and S_D are OFF (as shown in Figure 4b), and the proposed IIABB converter operates according to the waveform during the time t_1–t_2, as shown in Figure 5. In mode 1, the V_o Equation (7) is as follows:

$$V_o = \frac{DV_{pv} - V_{DA}(1 - D)}{1 - D} 1 \cdot n \tag{7}$$
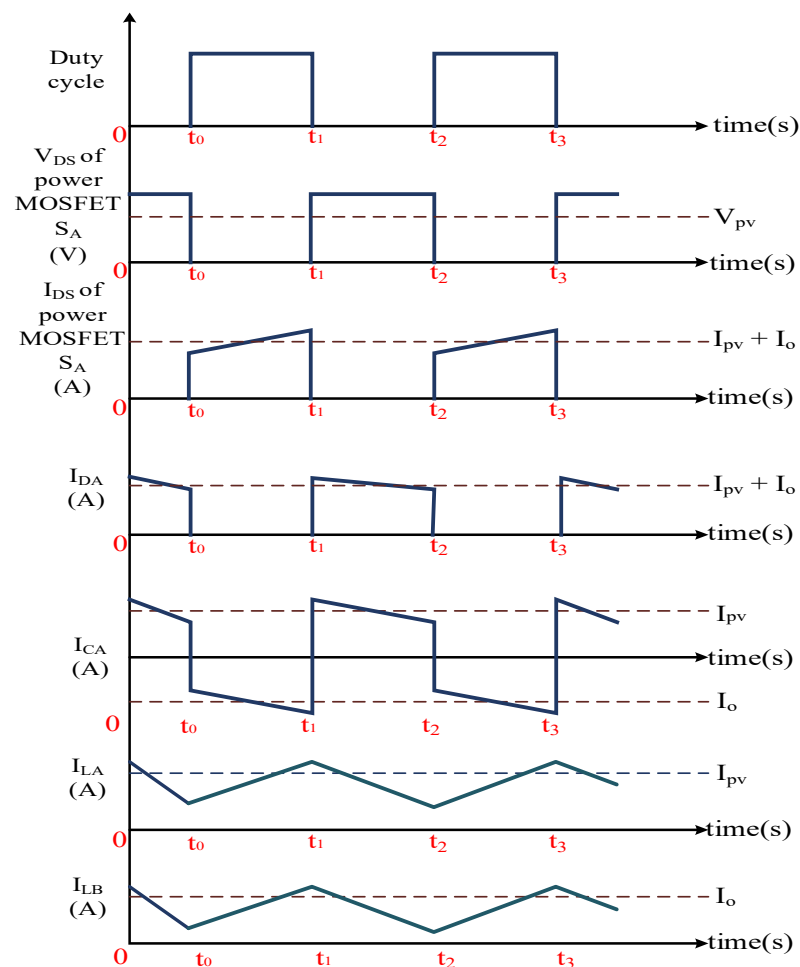

Figure 5. Voltage and current waveforms show V_{DS}, I_{DS}, I_{DA}, I_{CA}, I_{LA}, and I_{LB} along with the duty cycle of the proposed IIABB converter.

Equation (8) also applies to the magnetizing inductor L_{MB} from inductor L_B, whose current begins to increase when V_{CA} is applied.

$$I_{LMB}(t) = \frac{V_{pv}(t_1 - t_0)}{L_{MB}} + I_{LMB}(0) \tag{8}$$

It is during this mode that the load current is supplied by the output capacitor.

From the time t_{21}–t_2, the switch S_A is not conducting a rectifying diode, and a coupled inductor will convert the energy stored in L_{MA} and L_{MB} into an output. According to Equations (9) and (10) below, the current on L_{MA} and L_{MB} will decrease when the voltage polarity is reversed on them.

$$I_{LMA}(t) = I_{LMA}(t_1) - \frac{V_{DS} - V_{CA}}{L_{MA}}(t_2 - t_1) \tag{9}$$

$$I_{LMB}(t) = I_{LMB}(t_1) - \frac{V_{DS} - V_{CA}}{L_{MB}}(t_2 - t_1) \tag{10}$$

One operating period ends, and a similar one begins in the time interval t_2. Figure 5 illustrates the key waveforms of the proposed IIABB converter.

In mode 2, the power MOSFET S_A is ON and the power MOSFETs S_B, S_C, and S_D are OFF (as shown in Figure 4a), and the proposed IIABB converter operates according to the waveform during time t_0–t_1 as shown in Figure 5. In the next interval of the proposed IIABB converter, the power MOSFET S_C is ON and the power MOSFETs S_A, S_B, and S_D are OFF (as shown in Figure 4c), and the proposed IIABB converter operates according to the waveform during time t_1–t_2 as shown in Figure 5. The output voltage V_o can be calculated with the help of Equation (11) below:

$$V_o = \frac{DV_{pv} - V_{DA}(1 - D)}{1 - D} 2 \cdot n \tag{11}$$

Similarly, in mode 3, the power MOSFET S_A is ON. The rest of the switches S_B, S_C, and S_D are turned OFF (as shown in Figure 4a), and the proposed IIABB converter operates according to the waveform during time t_0–t_1 (Figure 5). In the next interval of the proposed IIABB converter, the power MOSFET S_D is ON and the power MOSFETs S_A, S_B, and S_C are OFF (as shown in Figure 4d), and the proposed IIABB converter operates according to the waveform during time t_1–t_2 (as shown in Figure 5). The output voltage V_o can be calculated with the help of Equation (12) below:

$$V_o = \frac{DV_{pv} - V_{DA}(1 - D)}{1 - D} 3 \cdot n \tag{12}$$

3.2. Topology Analysis

The proposed IIABB converter scheme is shown in Figure 4. The converter is at steady state, which implies that all currents and voltages are of a periodic nature, starting and ending at the same points over the whole switching period, and operating in current conduction mode (CCM).

The solar PV simulator output voltage V_{pv} and the DC blocking capacitor C_A are considered constants. D is the duty ratio of the switch, DT is the period in which the switch is closed, and $(1 - D)T$ is the period during which it is open.

Take ideal conditions into account: when the switch S_A is open, the diode is ON, and Kirchhoff's voltage law applies as follows:

$$V_{LA} = V_{pv} \tag{13}$$

$$V_{CA} - \frac{V_o}{N \cdot n} = 0 \tag{14}$$

$$V_{CA} = \frac{V_o}{N \cdot n} \tag{15}$$

When the switch S_A is closed, the diode is OFF. The voltage across L_A for the interval DT is as follows:

$$V_{pv} - V_{LA} - \frac{V_o}{N \cdot n} = 0 \tag{16}$$

Kirchhoff's voltage law around the path containing V_{pv}, V_{LA}, and V_{CA} gives the following:

$$V_{pv} - V_{LA} + V_{CA} - \frac{V_o}{N \cdot n} = 0 \tag{17}$$

$$V_{LA} = V_{pv} + V_{CA} - \frac{V_o}{N \cdot n} = 0 \tag{18}$$

$$V_{LMA} = V_{CA} \tag{19}$$

$$V_{LMA} = \frac{V_o}{N \cdot n} \tag{20}$$

$$V_{pv}D + (V_{pv} + V_{CA} - \frac{V_o}{N \cdot n})(1 - D) = 0 \tag{21}$$

$$V_{pv} + V_{CA}(1 - D) = \frac{V_o}{N \cdot n}(1 - D) = 0 \tag{22}$$

$$V_{CA}(1 - D) + \frac{V_o}{N \cdot n}(1 - D)^2 = 0 \tag{23}$$

$$V_{CA}(1 - D) + \frac{V_o}{N \cdot n \cdot D}(1 - D)^2 = 0 \tag{24}$$

$$V_{CA}(1 - D) = \frac{-V_o}{N \cdot n \cdot D}(1 - D)^2 \tag{25}$$

$$V_{pv} - \frac{V_o}{N \cdot n \cdot D}(1 - D)^2 = \frac{V_o}{N \cdot n \cdot D}(1 - D) \tag{26}$$

$$V_{pv} = \frac{V_o}{N \cdot n \cdot D}(1 - D)^2 + \frac{V_o}{N \cdot n \cdot D}(1 - D) \tag{27}$$

$$V_{pv} = \frac{V_o(1 - D)^2 + V_o(1 - D)}{N \cdot n \cdot D} \tag{28}$$

$$\frac{V_{pv}}{(1 - D)} = \frac{V_o(1 - D) + V_o D}{N \cdot n \cdot D} \tag{29}$$

Equation (30) for voltage gain switch voltage stress is as follows:

$$V_o = \frac{D V_{pv}}{1 - D} N \cdot n \tag{30}$$

where D is the duty cycle of the switch and 'n' is the turn ratio considered to be (1:1).

3.3. Hill-Climbing Algorithm

The hill-climbing (HC) algorithm is the MPPT algorithm often used in solar power systems. This is because of the HC algorithm's simple control structure and low design cost. The HC algorithm is suitable for a uniform sunlight environment, and this algorithm is compared according to the output power of solar PV modules to control the actuating point and then catch the MPP. This algorithm's disadvantages [25–27] are as follows:

(1) With its disturbance characteristics, it will cause power loss and lower the system's performance.
(2) It is not suitable for partially shaded environments; it will operate at the local maximum power point, resulting in low system efficiency.

This study proposes an IIABB converter combined with the HC algorithm. The proposed IIABB converter is verified to be suitable for the MPPT algorithm under actual measurements so that the solar power generation system can capture MPP and improve system performance.

4. Simulation and Experimental Results

Simulation Result

The proposed IIABB converter is simulated in MATLAB R2021b at different input voltages, and the results are being compared with the conventional SEPIC converter. The parameters/components specifications used in MATLAB for the novel SEPIC converter are shown in Table 1. The proposed IIABB converter gives a constant output voltage V_o, irrespective of the solar PV module output voltage V_{pv}.

Some of the conditions are discussed below:

Condition 1:

Figure 6 shows the simulation waveform of the proposed IIABB converter for solar PV module output voltage V_{pv} of 20 V and N = 1. Figure 6a shows the switching modulation of the gate pulse of four switches by showing that switches S_A and S_B are in conduction mode whereas S_C and S_D are not conducting, and the duty cycle of the power MOSFET S_A is calculated to be 0.7 by choosing the value of N = 1 with the help of Equation (7).

When the solar PV module output voltage of V_{pv} 20 V is applied with a duty cycle of 0.7, an output voltage of 48 V is achieved, as shown in Figure 6b for the use of battery charge.
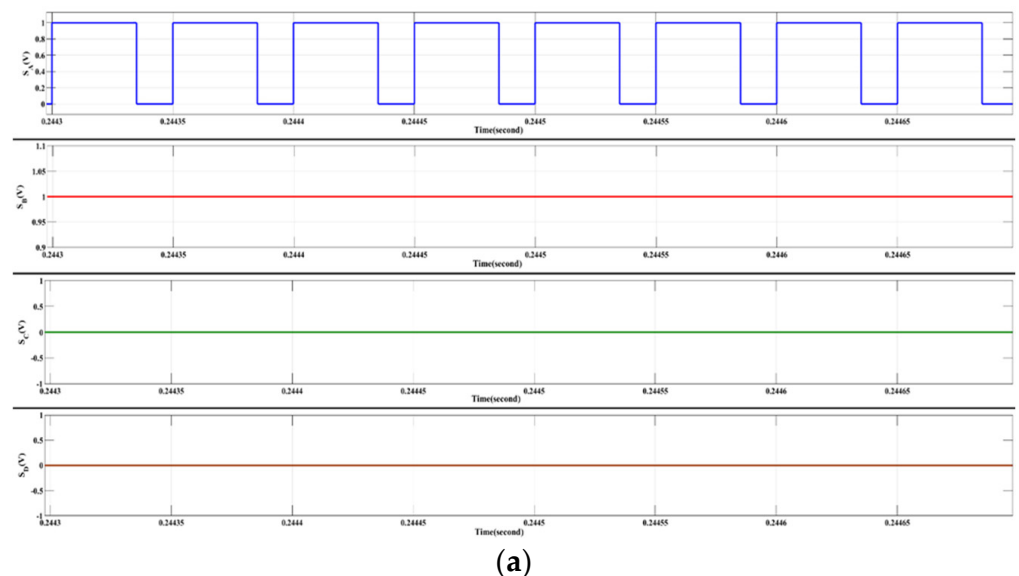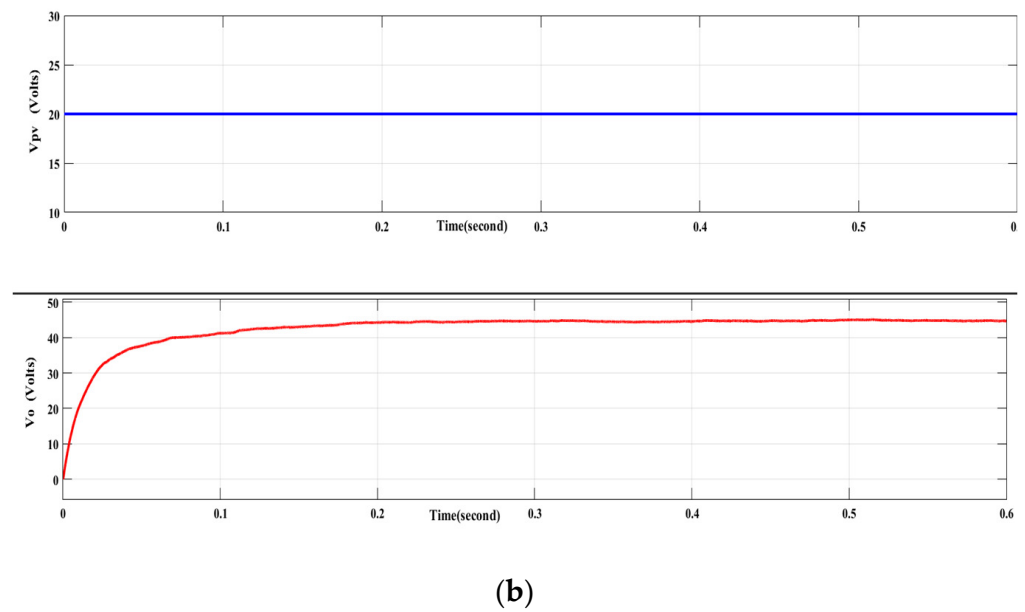

(a)

Figure 6. *Cont.*

(b)

Figure 6. Simulation result of the proposed IIABB converter for solar PV module input voltage V_{pv} of 20 V and corresponding output voltage V_o = 48 V and number of connected inductors N = 1 with duty cycle 0.7 (**a**) gate pulse waveform where S_A and S_B are in operating condition and S_C and S_D are not operating, and (**b**) the V_{pv} and output voltage V_o.

Condition 2:

Figure 7 shows the simulation results of the proposed IIABB converter for V_{pv} of 20 V and N = 2. Figure 7a shows the switching modulation of the gate pulse of four switches with switches S_A and S_C in conduction mode, whereas S_B and S_D are not conducting, and the duty cycle of the power MOSFET S_A is calculated to be 0.55 by choosing the value of N = 2 with the help of Equation (11). When V_{pv} = 20 V is applied with a duty cycle of 0.55, an output voltage of 48 V is achieved, as shown in Figure 7b for the use of battery charge.
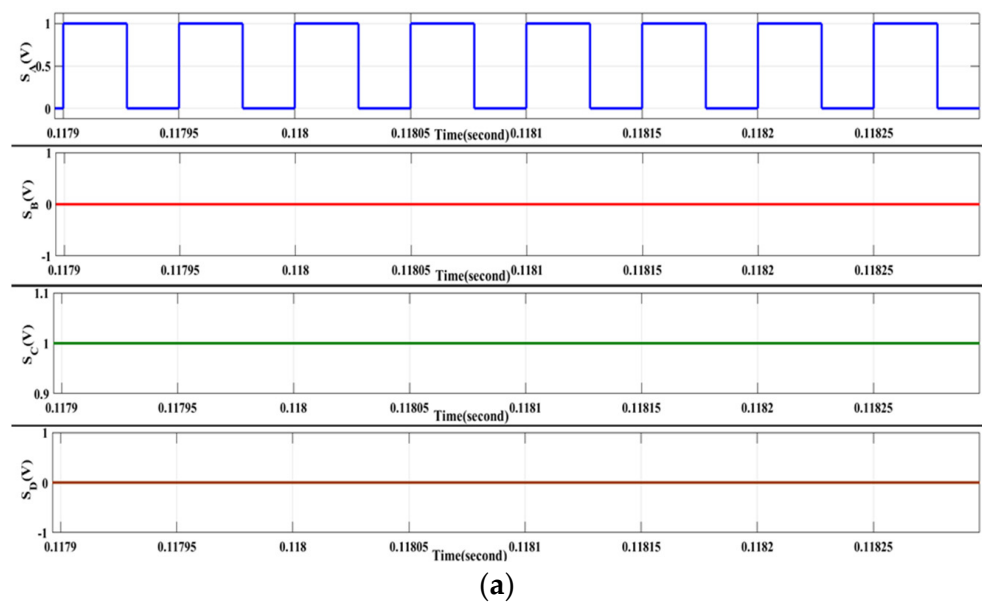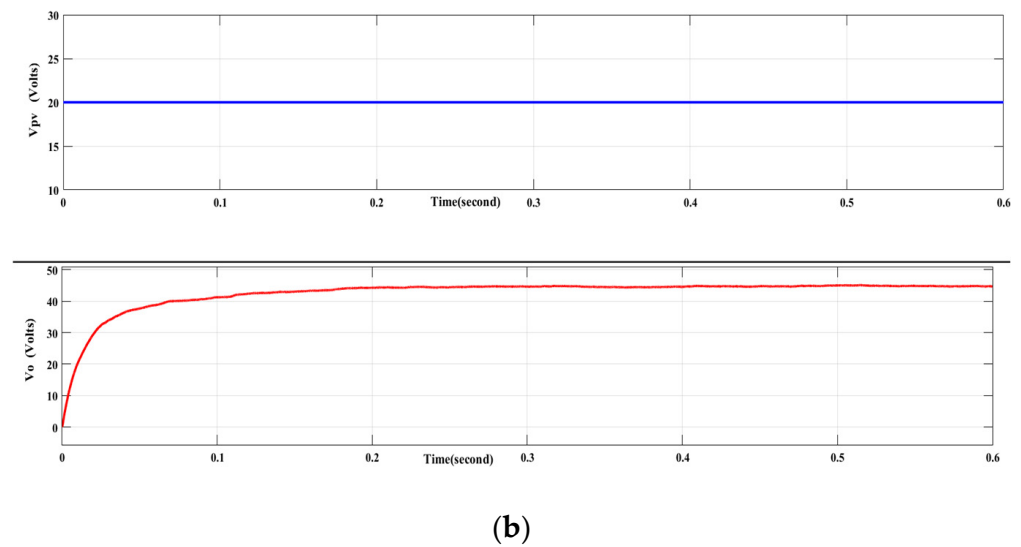

(a)

Figure 7. *Cont.*

(b)

Figure 7. Simulation result of the proposed IIABB converter for solar PV module input voltage V_{pv} of 20 V and corresponding output voltage V_o = 48 V and number of connected inductors N = 2 with duty cycle 0.55 (**a**) gate pulse waveform where S_A and S_C are in operating condition and S_B and S_D are not operating, and (**b**) the V_{pv} and output voltage V_o.

Condition 3:

Figure 8 depicts the simulation results of the proposed IIABB converter for V_{pv} of 30 V and N = 3. Figure 8a shows the switching modulation of the gate pulse of four switches with switches S_A and S_D in conduction mode, whereas S_B and S_C are not conducting, and the duty cycle of the power MOSFET S_A is calculated to be 0.35 by choosing the value of N = 3 with the help of Equation (12). When V_{pv} = 30 V is applied with a duty cycle of 0.35, an output voltage of 48 V is achieved, as shown in Figure 8b.
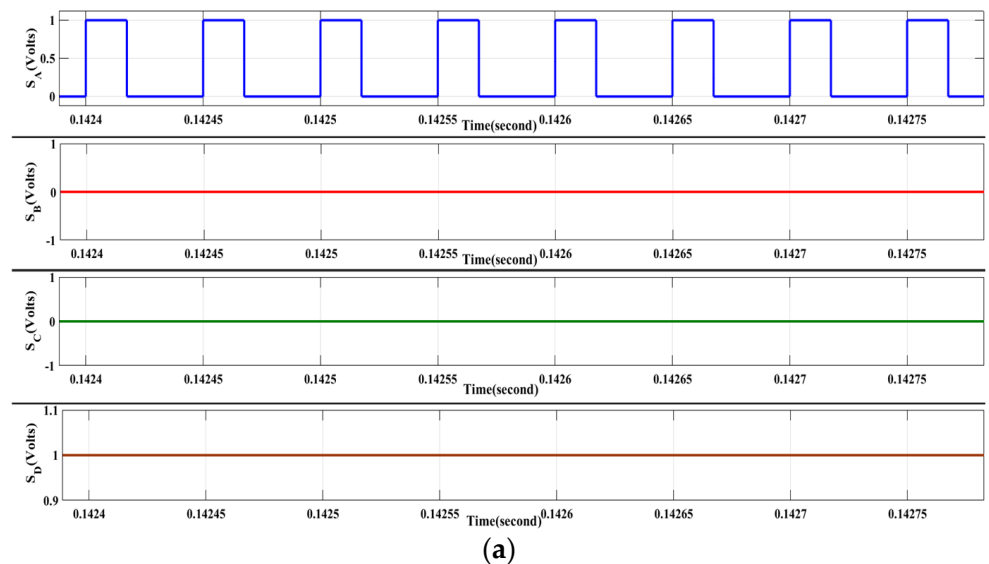

(a)
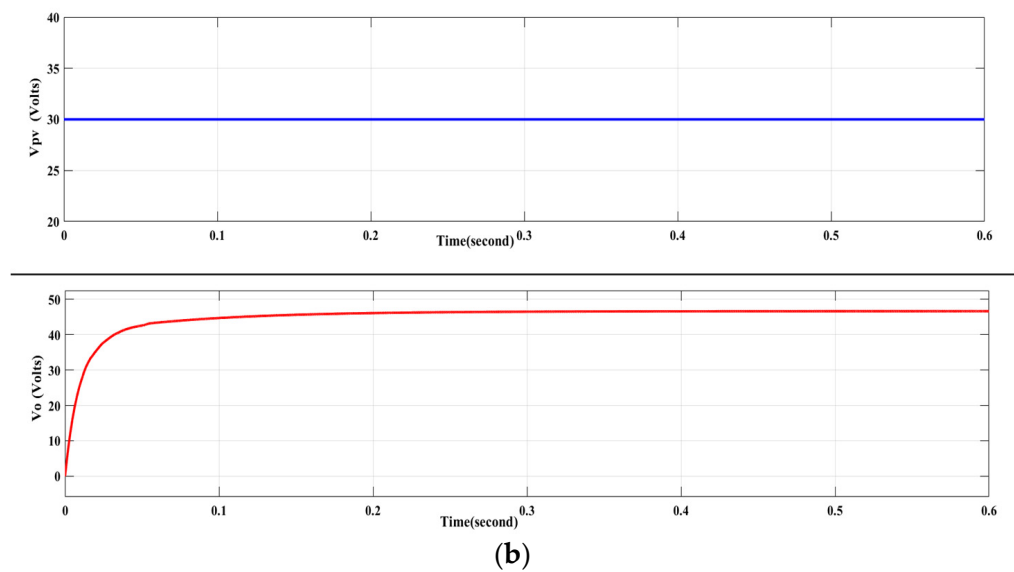
Figure 8. *Cont.*

(b)

Figure 8. Simulation result of the proposed IIABB converter for solar PV module input voltage V_{pv} of 30 V and corresponding output voltage V_o = 48 V and number of connected inductors N = 3 with duty cycle 0.35 (**a**) gate pulse waveform where S_A and S_D are in operating condition and S_B and S_C are not operating, and (**b**) the V_{pv} and output voltage V_o.

Table 2 illustrates the proposed topology compared with conventional SEPIC and boost converters, previous non-coupled inductor SEPIC-based converters [27,28], and other previous converters that employ the same topology. With reference to the other literature, this comparison compares the voltage gain capability of the proposed converter. It can be seen from the table that the voltage gain of the proposed converter is higher than those in [27–29] and also than the SEPIC and boost converters, both used in classical electronics. A continuous input current is also provided by the converter. Consequently, renewable energy applications will be easier to implement. Accordingly, the proposed converter has the advantages of coupled inductor converters and also has a high voltage gain, low voltage stress on the elements, a continuous input current, a positive output, and is capable of handling more power in comparison with the converters with near voltage gains in [28,30]. With the help of Table 2, it becomes clear that with a low duty ratio, the gain will be high and hence more efficient when compared to other topologies.

Table 2. Comparison between the proposed converter and some other converters.

References	Parameters				
	Voltage Gain	Number of Switches	Number of Diodes	Number of Inductors	Continous Input Current
Proposed	$\dfrac{DV_{pv}}{1-D}N \cdot n$	4	2	5	Yes
SEPIC	$\dfrac{D}{1-D}$	1	2	2	Yes
Boost	$\dfrac{D}{1-D}$	1	1	1	Yes
[27]	$\dfrac{1+D}{1-D}$	1	2	2	Yes
[28]	$\dfrac{3D}{1-D}$	1	2	2	Yes
[29]	$\dfrac{2D}{1-D}$	1	2	2	No
[30]	$\dfrac{-3D}{1-D}$	1	3	3	No

For the purpose of verifying the theoretical analysis and effectiveness of the proposed IIABB converter, a laboratory prototype of the converter is implemented and tested in conjunction with the previous section. The proposed IIABB converter specification is shown in Table 1. The above simulation results were verified by hardware implementation. Figure 9 illustrates the experimental setup of the proposed converter. For controlling the novel converter, the Texas DSP TMS320F28379D is used as a pulse width modulation IC. In Table 3, the solar PV simulator specifications are under an irradiance level of 1000 W/m^2 and a temperature of 25 °C; we have taken 50 V and 5.5 A for the open circuit voltage and short circuit current, respectively, and 200 W as the maximum power achieved.
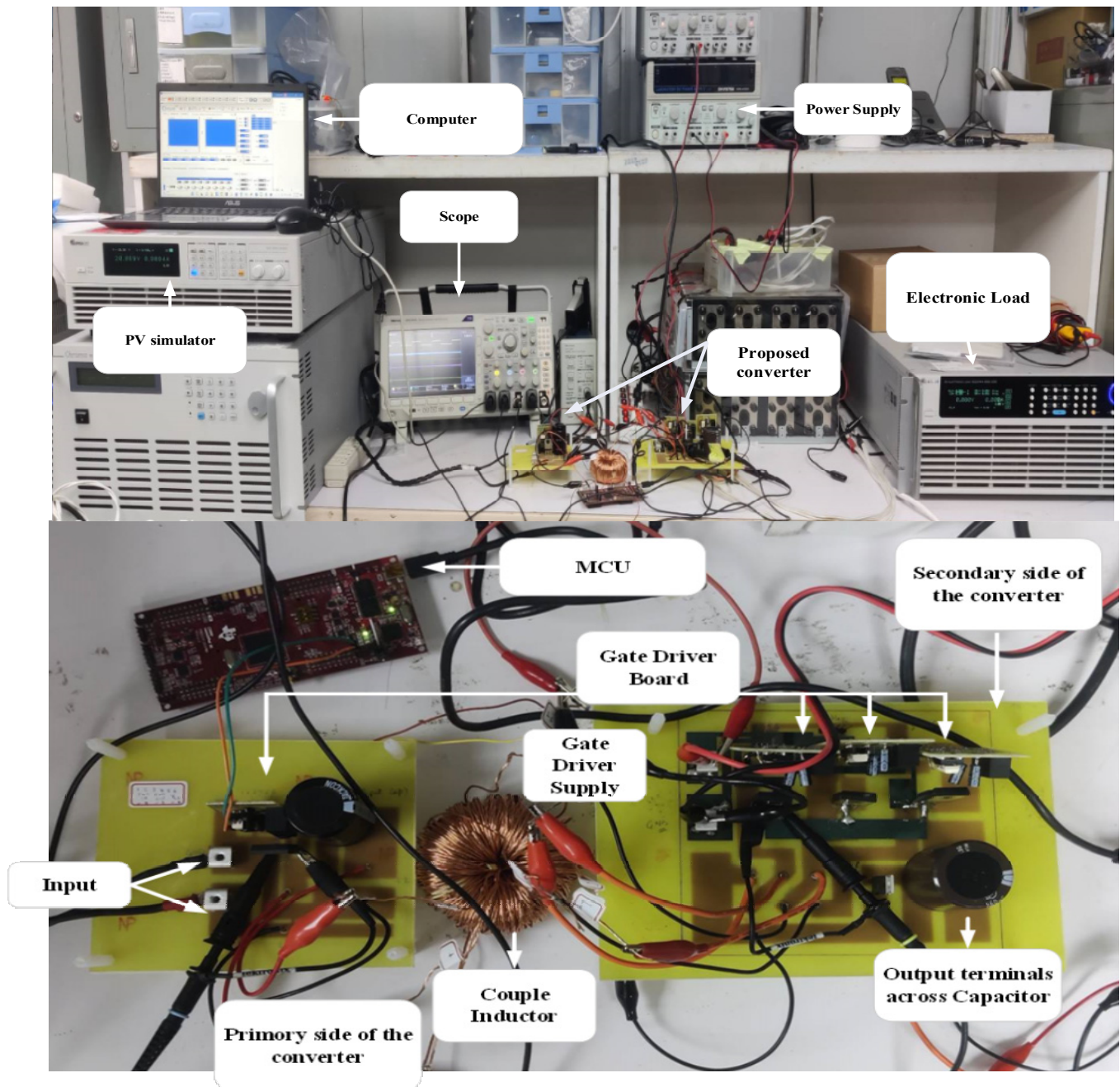

Figure 9. Hardware prototype of the proposed IIABB converter.

Table 3. The solar PV simulator specification.

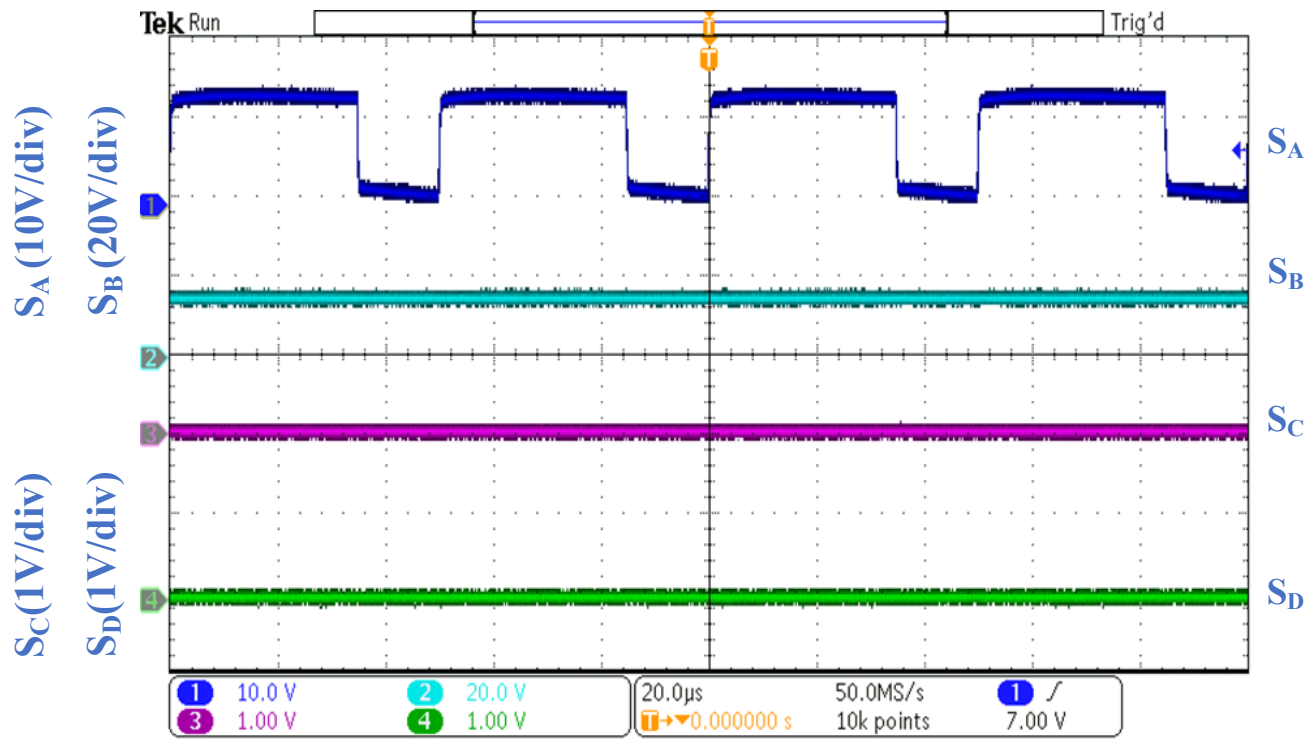| Parameters	Specification
Open circuit voltage (V_{oc})	50 V
Short circuit current (I_{sc})	5.5 A
Maximum power point voltage (V_{mpp})	40 V
Maximum power point current (I_{mpp})	5 A
Maximum power point (P_{mpp})	200 W

Table 4 illustrates the hardware results for the proposed IIABB converter by varying the number of inductors (N) along with the solar PV simulator output voltage V_{pv} and the constant output voltage variation because a battery charger requires constant output voltage with various advantages. As the number of inductors increases, the current ripple of the proposed converter reduces, providing high gain with a low duty ratio when compared to a conventional SEPIC converter. Moreover, the coupled inductor reduces the size of the whole circuitry.

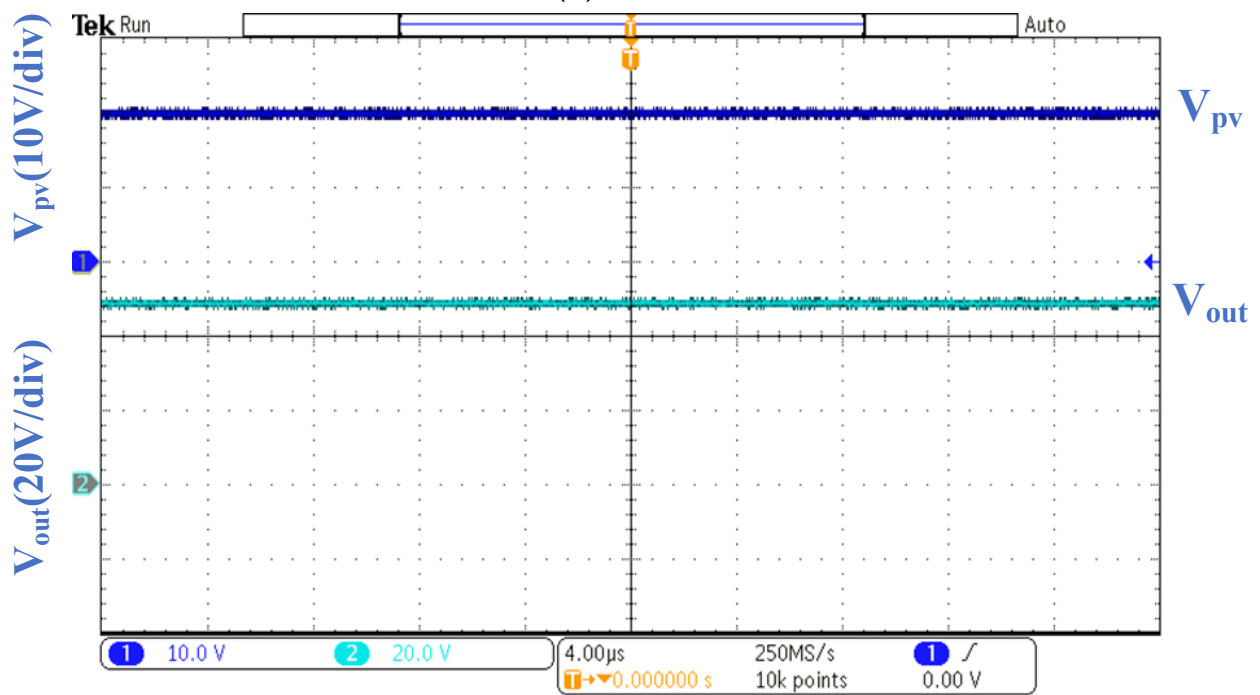**Table 4.** Hardware results for the proposed IIABB converter for battery charger application.

Number of Inductors	V_{pv}	V_o	D	Efficiency
	20 V	48 V	0.70	92%
N = 1	30 V	48 V	0.62	94%
	40 V	48 V	0.55	96%
	20 V	48 V	0.55	96%
N = 2	30 V	48 V	0.47	98%
	40 V	48 V	0.38	99%
	20 V	48 V	0.45	98%
N = 3	30 V	48 V	0.35	99%
	40 V	48 V	0.30	99%

Figure 10 shows the experimental waveform of the proposed IIABB converter for a V_{pv} of 20 V and number of inductors N = 1. Figure 11a displays the switches S_A and S_B are operating, while S_C and S_D are not operating, and the switches work via an intelligent control strategy. Figure 11b shows the waveform of V_{pv} = 20 V and an output voltage of V_{out} = 48 V at a duty cycle of 0.7 according to Equation (5). Figure 11 shows the experimental waveform of the proposed IIABB converter for a V_{pv} of 30 V and N = 1. Figure 12a displays the switches S_A and S_B are operating; the switches S_C and S_D are not operating via an intelligent control strategy. Figure 12b shows the waveform of V_{pv} = 20 V and an output voltage of V_{out} = 48 V at a duty cycle of 0.62 according to Equation (5), as shown in Table 4.

Figures 12–14 show an irradiance level of 1000 W/m^2 and a temperature of 25 °C, the experimental waveform of the proposed IIABB converter, and N = 1, 2, and 3, respectively. In these cases, the proposed IIABB converter has an intelligent control strategy and HC algorithm. First, switch S_A works by the HC algorithm. Second, switches S_B, S_C, and S_D work via an intelligent control strategy. Finally, V_{pv} = 40 V, i.e., the HC algorithm, catches the maximum power point voltage V_{mpp}, and V_{out} = 48 V can offer battery charging, as shown in Table 4.

(**a**)

(**b**)

Figure 10. Experimental waveforms of the proposed IIABB converter for V_{pv} of 20 V and N = 1: (**a**) experimental waveforms of switches S_A and S_B are operating; S_C and S_D are not operating; and (**b**) waveforms of V_{pv} = 20 V and output voltage V_{out} = 48 V via an intelligent control strategy at a duty cycle of 0.7.
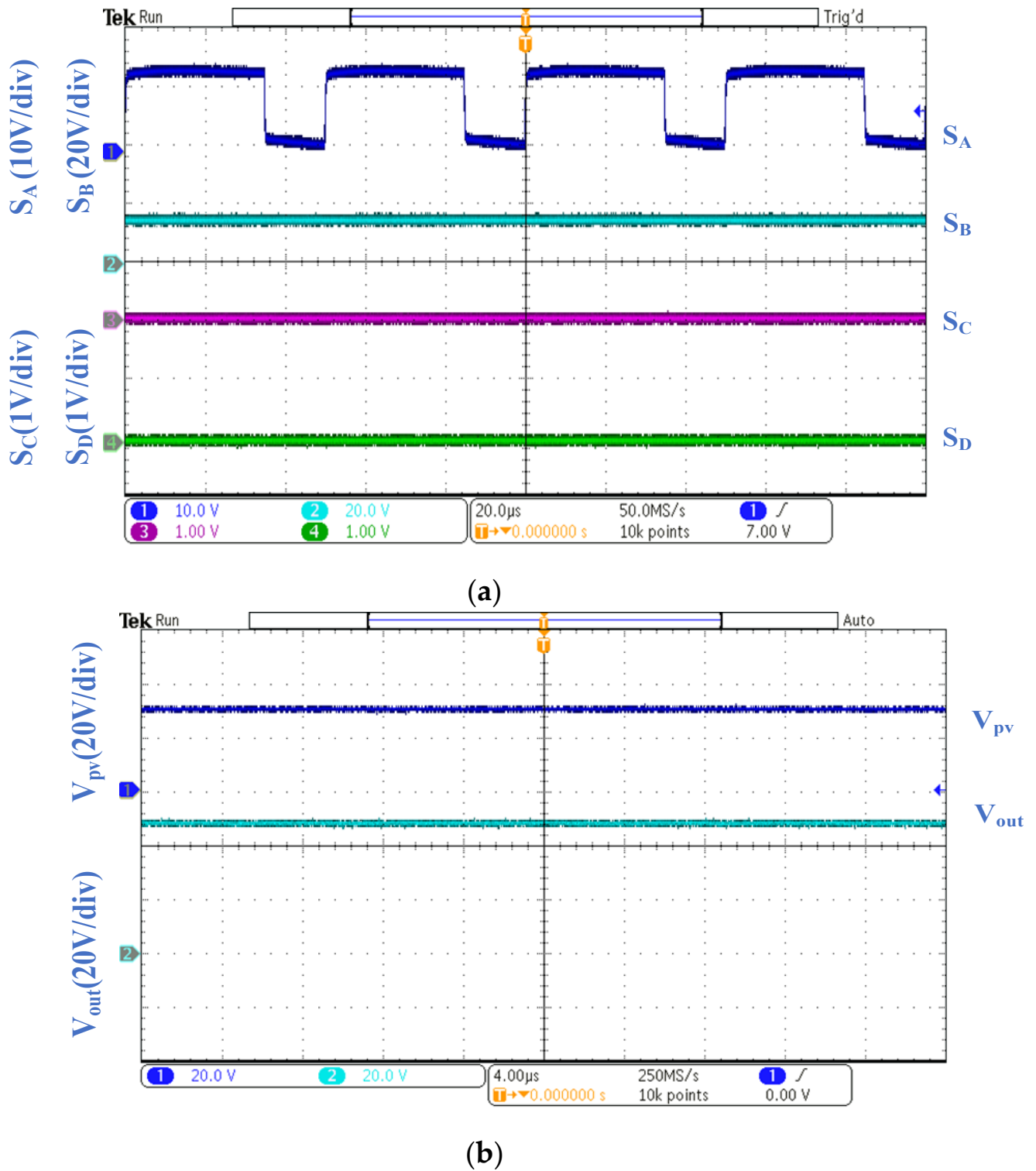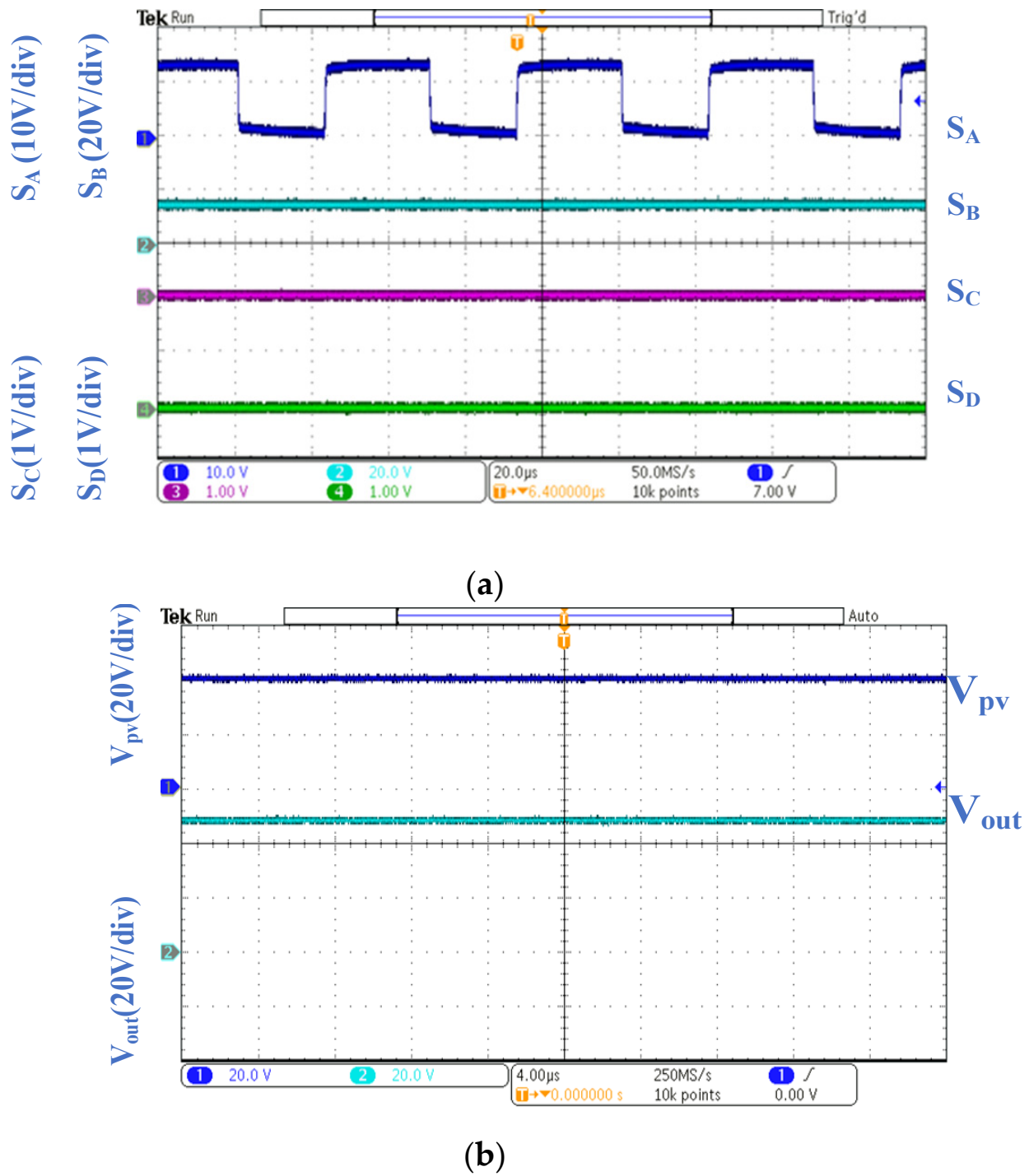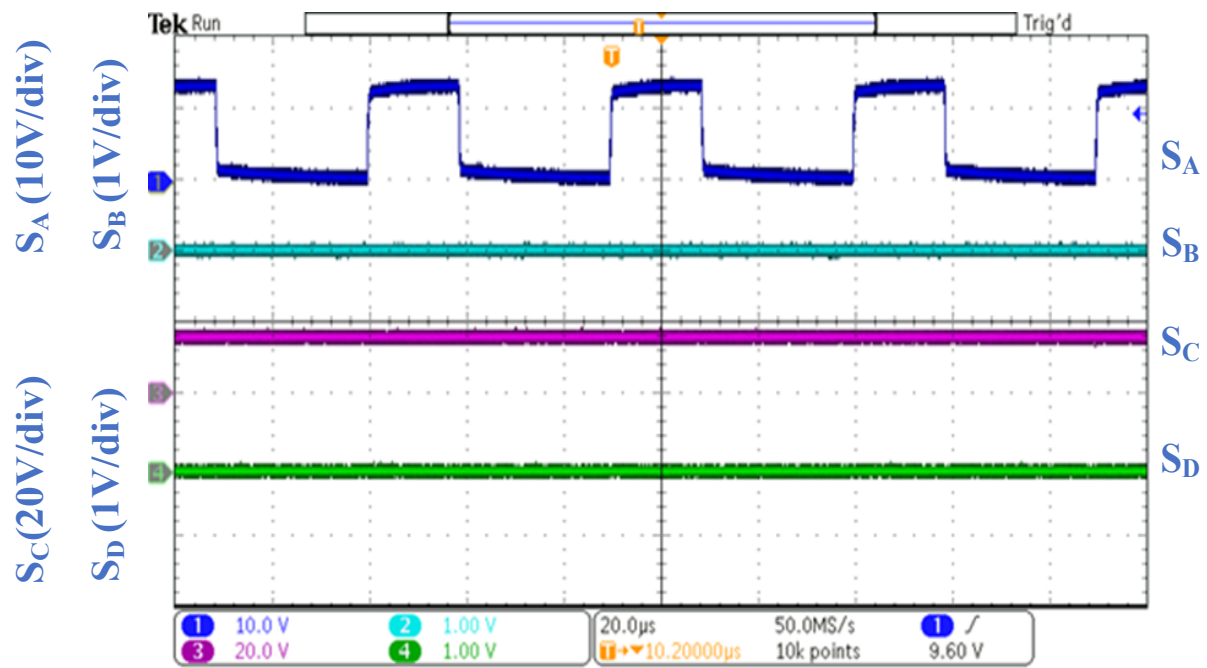
(**a**)

(**b**)

Figure 11. Experimental waveforms of the proposed IIABB converter for V_{pv} of 30 V and N = 1: (**a**) experimental waveforms of switches S_A and S_B that are operating; S_C and S_D are not operating; and (**b**) waveforms of V_{pv} = 30 V and output voltage V_{out} = 48 V via an intelligent control strategy at a duty cycle of 0.62.
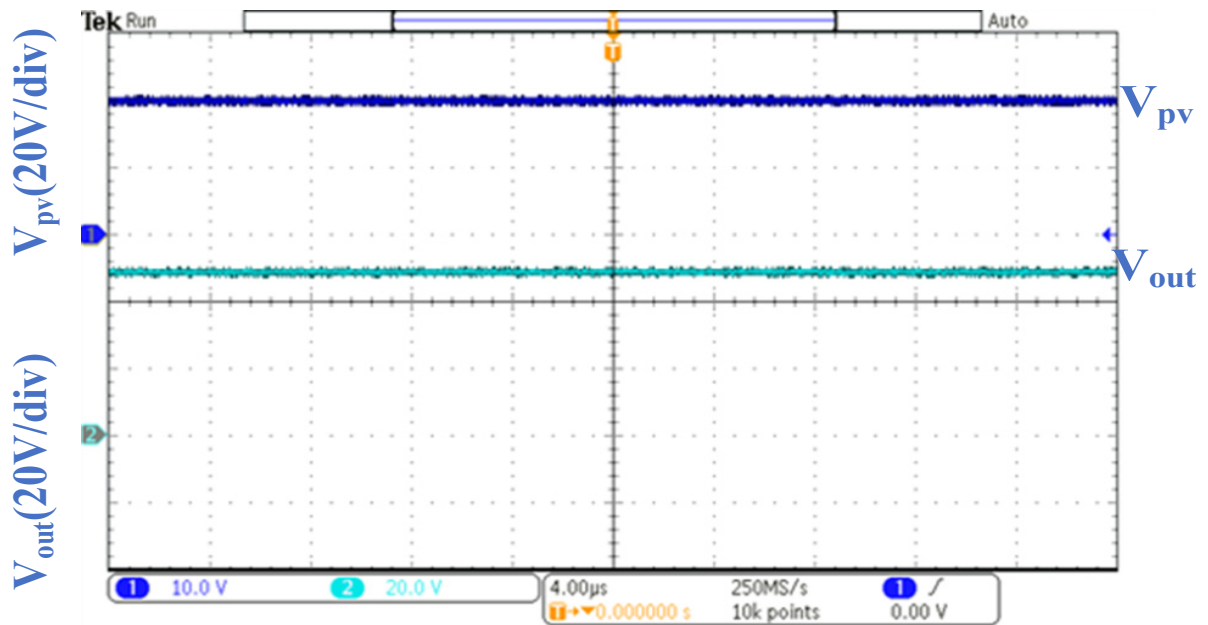
(**a**)

(**b**)

Figure 12. Experimental waveforms of the proposed IIABB converter for V_{pv} of 40 V and N = 1: (**a**) experimental waveforms of switches S_A and S_B are operating; S_C and S_D are not operating; and (**b**) waveforms of V_{pv} = 40 V and output voltage V_{out} = 48 V via an intelligent control strategy and HC MPPT algorithm at a duty cycle of 0.55.

(**a**)

(**b**)

Figure 13. Experimental waveforms of the proposed IIABB converter for V_{pv} of 40 V and N = 2: (**a**) experimental waveforms of switches S_A and S_C are operating; S_B and S_D are not operating; and (**b**) waveforms of V_{pv} = 40 V and output voltage V_{out} = 48 V via an intelligent control strategy and HC MPPT algorithm at a duty cycle of 0.38.
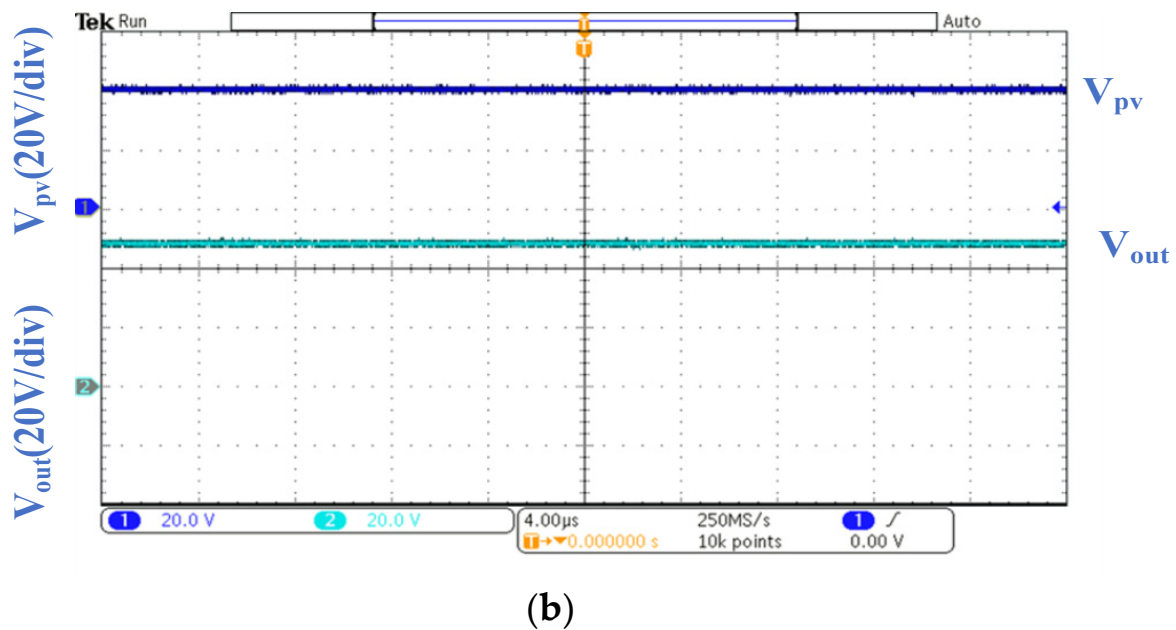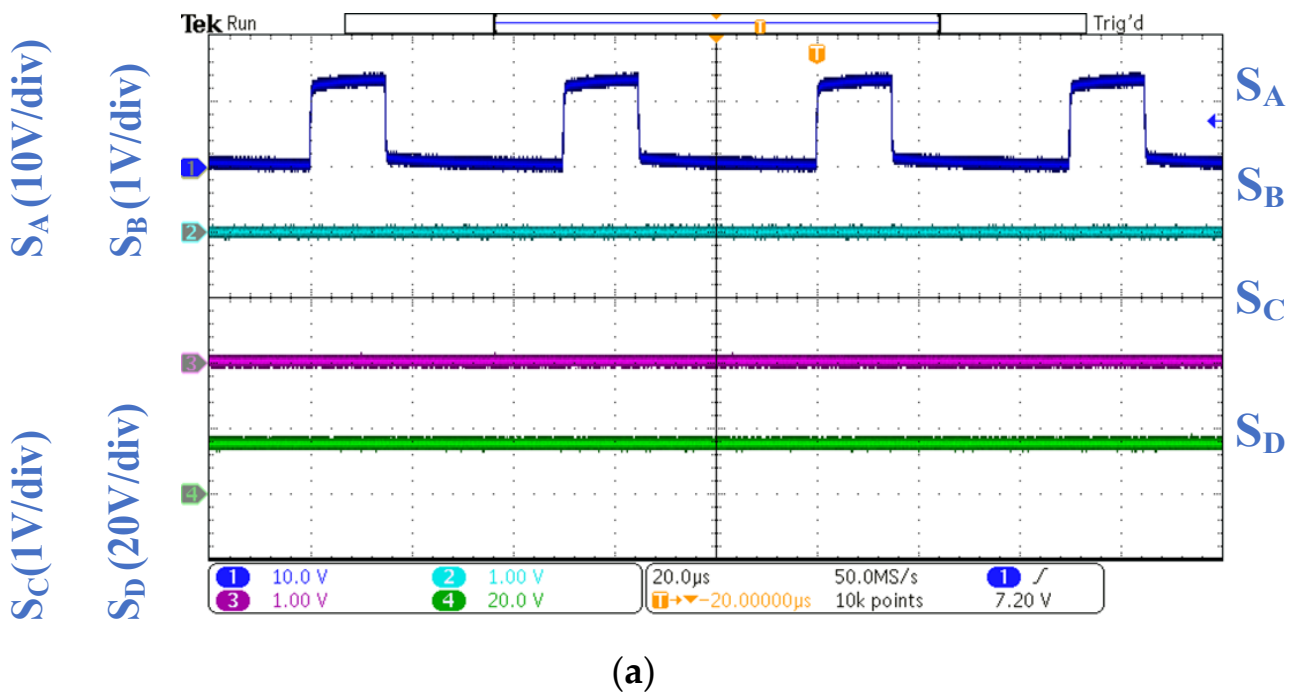
(a)

(b)

Figure 14. Experimental waveforms of the proposed IIABB converter for V_{pv} of 40 V and N = 3: (**a**) experimental waveforms of switches S_A and S_D are operating; S_B and S_C are not operating; and (**b**) waveforms of V_{pv} = 40 V and output voltage V_{out} = 48 V via an intelligent control strategy and HC MPPT algorithm at a duty cycle of 0.3.

5. Conclusions

This study has presented a detailed description and circuit design, as well as step-by-step design equations for the proposed IIABB converter for a solar power system. The proposed converter has a constant output voltage and can be utilized with an intelligent control strategy and HC MPPT algorithm to capture the MPP. With the help of MATLAB

R2021, the performance of the innovative IIABB converter is compared and verified with the performance of the conventional SEPIC converter. Instead of a transformer, a coupled inductor is designed, which significantly reduces the input current ripple of the converter and hence reduces the cost and size of the converter. Simulation results and experimental results revealed that the proposed converter is more efficient than conventional DC–DC converters at various input voltage levels and gives high efficiency at low duty cycles. In addition, we use the HC algorithm for MPPT control, which improves the system's performance. The proposed IIABB converter efficiency is ~92–99%. In this case, we have taken an electronic load in CC (constant current) mode. When the load changes, the load current will change, and output can control voltage level from the load terminal.

This research has contributed to the development of a novel IIABB converter that may be employed in renewable energy systems. The constant output voltage of the novel converter can be used for battery charging and for inverter applications; therefore, the proposed converter is suitable for various conditions.

In the future, we can increase the number of components in the proposed IIABB converter so that it can be used for high-power applications, such as for large industrial purposes and numerous PV applications; moreover, by making some minor changes in the circuitry, a new form of DC–AC inverter can also be proposed with the help of this same idea.

Author Contributions: Conceptualization, B.S., H.-D.L. and C.-H.L.; Formal analysis, B.S. and H.-D.L.; Investigation, B.S. and H.-D.L.; Methodology, B.S., H.-D.L. and C.-H.L.; Supervision, H.-D.L.; Writing—original draft, B.S., H.-D.L., C.-H.L., S.-D.L., A.S. and L.-Y.H.; Writing—review & editing, B.S., H.-D.L., C.-H.L., S.-D.L., A.S. and L.-Y.H. All authors provided critical feedback and helped with the research and analysis of the manuscript. All authors have read and agreed to the published version of the manuscript.

Data Availability Statement: Not applicable.

References

1. Meena Devi, R.; Geetha, V.; Meenakshi, V. Speed Control of SEPIC Converter-Based Induction Motor Drive System. In *Emerging Solutions for e-Mobility and Smart Grids*; Springer: Singapore, 2021; pp. 15–23. [CrossRef]
2. Nguimfack-Ndongmo, J.D.D.; Kenné, G.; Kuate-Fochie, R.; Tchouani Njomo, A.F.; Mbaka Nfah, E. Adaptive neuro-synergetic control technique for SEPIC converter in PV systems. *Int. J. Dyn. Control* **2022**, *10*, 203–216. [CrossRef]
3. Sivamani, D.; Ramkumar, R.; Ali, A.N.; Shyam, D. Design and implementation of highly efficient UPS charging system with single-stage power factor correction using SEPIC converter. *Mater. Today Proc.* **2021**, *45*, 1809–1819. [CrossRef]
4. Faizan, M.; Sabir, B.; Tahir, M.; Rahman, K.; Ashraf, I. Analysis of Five Level H-Bridge Inverter Using Bipolar Switching Schemes. In Proceedings of the 2021 International Conference on Computer Communication and Informatics (ICCCI), Coimbatore, India, 27–29 January 2021; pp. 1–6. [CrossRef]
5. Maroti, P.K.; Padmanaban, S.; Holm-Nielsen, J.B.; Bhaskar, M.S.; Meraj, M.; Iqbal, A. A new structure of high voltage gain SEPIC converter for renewable energy applications. *IEEE Access* **2019**, *7*, 89857–89868. [CrossRef]
6. Maroti, P.K.; Esmaeili, S.; Iqbal, A.; Meraj, M. High step-up single switch quadratic modified SEPIC converter for DC microgrid applications. *IET Power Electron.* **2020**, *13*, 3717–3726. [CrossRef]
7. Mosconi Ewerling, M.V.; Brunelli Lazzarin, T.; Illa Font, C.H. Proposal of an Isolated Two-Switch DC-DC SEPIC Converter. In Proceedings of the 2019 IEEE 15th Brazilian Power Electronics Conference and 5th IEEE Southern Power Electronics Conference (COBEP/SPEC), Santos, Brazil, 1–4 December 2019; pp. 1–6. [CrossRef]
8. Natchimuthu, S.; Chinnusamy, M.; Mark, A.P. Experimental investigation of PV based modified SEPIC converter fed hybrid electric vehicle (PV-HEV). *Int. J. Circ. Theor. Appl.* **2020**, *48*, 980–996. [CrossRef]
9. Majstorović, M.; Mršević, D.; Đurić, B.; Milešević, M.; Stević, Z.; Despotović, Ž.V. Implementation of MPPT Methods with SEPIC Converter. In Proceedings of the 2020 19th International Symposium INFOTEH-JAHORINA (INFOTEH), East Sarajevo, Bosnia and Herzegovina, 18–20 March 2020; pp. 1–6. [CrossRef]

10. Mouslim, S.; Kourchi, M.; Ajaamoum, M. Simulation and analyses of SEPIC converter using linear PID and fuzzy logic controller. *Mater. Today Proc.* **2020**, *27*, 3199–3208. [CrossRef]

11. Kravetz, F.I.; Gules, R. Soft-Switching High Static Gain Modified SEPIC Converter. *IEEE J. Emerg. Sel. Top. Power Electron.* **2021**, *9*, 6739–6747. [CrossRef]

12. Sivaramkrishnan, M.; Marthanda, A.V.G.A.; Prasad, K.L.; Mujeer, S.A.; Durairaj, U.; Salim, M. Simulation of PV and WECS using CUK and SEPIC converter. In Proceedings of the 2021 5th International Conference on Intelligent Computing and Control Systems (ICICCS), Madurai, India, 6–8 May 2021; pp. 1–7. [CrossRef]

13. Kumari, R.; Pandit, M.; Sherpa, K. Modelling and Comparison of Conventional SEPIC Converter with Cascaded Boost–SEPIC Converter. *J. Inst. Eng. India Ser. B* **2021**, *102*, 99–109. [CrossRef]

14. Lu, S.-D.; Lin, C.-H.; Huang, L.-Y.; Lee, Y.-L.; Liu, H.-D.; Liao, P.-C.; Gao, G.-J.; Hsu, C.-M. Novel Global-MPPT Control Strategy Considering the Variation in the Photovoltaic Module Output Power and Loads for Solar Power Systems. *Processes* **2022**, *10*, 367. [CrossRef]

15. Balaji, C.; Anuradha, C.; Chellammal, N.; Bharadwaj, R. An extendable high-efficiency triple-port SEPIC–SEPIC converter with continuous input currents for DC microgrid applications. *Int. Trans. Electr. Energy Syst.* **2021**, *31*, e13121. [CrossRef]

16. Alili, A.; Camara, M.B.; Dakyo, B. Vienna Rectifier-Based Control of a PMSG Wind Turbine Generator. *Processes* **2022**, *10*, 413. [CrossRef]

17. Zunnurain, I.A.; Yumi, K.M.; Faisal, M.H. Performance Analysis of Single-Phase Inverter Using SEPIC Converter. In *Proceedings of the 6th International Conference on Electrical, Control and Computer Engineering*; Md. Zain, Z., Sulaiman, M.H., Mohamed, A.I., Bakar, M.S., Ramli, M.S., Eds.; Lecture Notes in Electrical Engineering; Springer: Singapore, 2022; Volume 842. [CrossRef]

18. Ghamari, S.M.; Gholizadeh-Narm, H.; Khavari, F. Robust Adaptive Controller Design for DC-DC SEPIC Converter in Photo Voltaic Application. In Proceedings of the 2019 6th International Conference on Control, Instrumentation and Automation (ICCIA), Sanandaj, Iran, 30–31 October 2019; pp. 1–6. [CrossRef]

19. Islam, N.; Mohammad, K.; Khan, R.A.; Sarwer, Z.; Sarwar, A. Symmetrical and Asymmetrical Multilevel Inverter Topologies with Reduced Device Count: A Review. In Proceedings of the 2nd International Conference for Emerging Technology (INCET), Belagavi, India, 21–23 May 2021; pp. 1–6. [CrossRef]

20. Yadav, A.; Verma, A. Modeling and Analysis of Modified SEPIC Converter Fed by Solar PV System. In Proceedings of the 2nd International Conference on Advances in Computing, Communication Control and Networking, Greater Noida, India, 18–19 December 2020; pp. 633–638. [CrossRef]

21. Nowdeh, S.A.; Moghaddam, M.J.H.; Babanezhad, M.; Davoodkhani, I.F.; Kalam, A.; Ahmadi, A.; Abdelaziz, A.Y. A novel maximum power point tracking method for photovoltaic application using secant incremental gradient based on Newton Raphson. In *Solar Photovoltaic Power Plants: Advanced Control and Optimization Techniques*; Springer: Singapore, 2019; pp. 71–96.

22. Arabi Nowdeh, S.; Moghaddam, M.J.H.; Nasri, S.; Abdelaziz, A.Y.; Ghanbari, M.; Faraji, I. A new hybrid moth flame optimizer-perturb and observe method for maximum power point tracking in photovoltaic energy system. In *Modern Maximum Power Point Tracking Techniques for Photovoltaic Energy Systems*; Springer: Cham, Switzerland, 2020; pp. 401–420.

23. Davoodkhani, F.; Nowdeh, S.A.; Abdelaziz, A.Y.; Mansoori, S.; Nasri, S.; Alijani, M. A New Hybrid Method Based on Gray Wolf Optimizer-Crow Search Algorithm for Maximum Power Point Tracking of Photovoltaic Energy System. In *Modern Maximum Power Point Tracking Techniques for Photovoltaic Energy Systems*; Springer: Cham, Switzerland, 2019; pp. 421–438.

24. Nasri, S.; Nowdeh, S.A.; Davoudkhani, I.F.; Moghaddam, M.J.H.; Kalam, A.; Shahrokhi, S.; Zand, M. Maximum power point tracking of photovoltaic renewable energy system using a new method based on turbulent flow of water-based optimization (TFWO) under Partial Shading Conditions. In *Fundamentals and Innovations in Solar Energy*; Springer: Singapore, 2021; pp. 285–310.

25. Lee, Y.-L.; Liu, H.-D. A Novel MPPT Heating Control Strategy Applied to the Induction Heating System. *Processes* **2022**, *10*, 1151. [CrossRef]

26. Liu, H.-D.; Lu, S.-D.; Lee, Y.-L.; Lin, C.-H. A Novel Photovoltaic Module Quick Regulate MPPT Algorithm for Uniform Irradiation and Partial Shading Conditions. *Processes* **2021**, *9*, 2213. [CrossRef]

27. Gules, R.; Santos, W.M.D.; Reis, F.A.D.; Romaneli, E.F.R.; Badin, A.A. A modified SEPIC converter with high static gain for renewable applications. *IEEE Trans. Power Electron.* **2014**, *29*, 5860–5871. [CrossRef]

28. Banaei, M.R.; Sani, S.G. Analysis and implementation of a new SEPIC-based single switch buck-boost dc-dc converter with continuous input current. *IEEE Trans. Power Electron.* **2018**, *33*, 10317–10325. [CrossRef]

29. Banaei, M.R.; Ardi, H.; Farakhor, A. Analysis and implementation of a new single-switch buck–boost DC/DC converter. *IET Power Electron.* **2014**, *7*, 1906–1914. [CrossRef]

30. Banaei, M.R.; Bonab, H.A.F. A novel structure for singleswitch nonisolated transformerless buck–boost DC–DC converter. *IEEE Trans. Ind. Electron.* **2017**, *64*, 198–205. [CrossRef]